Dynamics of cantilevered pipes conveying fluid. Part 3: Three-dimensional dynamics in the presence of an end-mass

Y. Modarres-Sadeghi, C. Semler, M. Wadham-Gagnon, M.P. Païdoussis*

Department of Mechanical Engineering, McGill University, 817 Sherbrooke St. West, Montréal, Québec, Canada H3A 2K6

Abstract

In this part, the last in a three-part study, the three-dimensional (3-D) dynamics of a cantilevered pipe conveying fluid is explored when an additional "point" mass is attached at the free end. For a typical case, the dynamical behaviour of this system is presented in the form of a bifurcation diagram, along with the time traces, phase-plane plots, PSD plots and Poincaré maps, showing planar periodic, quasiperiodic and chaotic oscillations, followed by 3-D quasiperiodic and chaotic motions. The effect on the results of the number of beam modes used in the Galerkin solution scheme is studied in some detail. The theoretical results are then compared with the results of a set of experiments done previously and good qualitative and quantitative agreement is observed.

1. Introduction

All the early experiments on plain cantilevered pipes conveying fluid (i.e., without additional masses attached to the pipe) showed that, for sufficiently high flow velocities, the system loses stability by flutter, and that the observed flutter remains in a plane (Païdoussis, 1963, 1970; Gregory and Païdoussis, 1966b; Bishop and Fawzy, 1976; Jendrzejczyk and Chen, 1985); refer also to Païdoussis (1998, Section 3.5.6). As a result, most of the theoretical work was done for planar motions of the pipe, starting with Gregory and Païdoussis (1966a), and even earlier by Bourrières (1939) and Benjamin (1961a,b).[1]

The first studies on pipes with attached masses were undertaken by Hill and Swanson (1970), Jendrzejczyk and Chen (1985) and Sugiyama et al. (1988); in the second of these studies, the attached mass was at the free end—here referred to as an "end-mass". The results obtained were sufficiently interesting to ensure continued study of the problem; e.g., the additional mass(es) could either stabilize or destabilize the system *vis-à-vis* the plain pipe, depending on the system parameters and location of the additional mass(es) [see Païdoussis (1998, Section 3.6.3)].

All of the theoretical work discussed so far has been conducted with the aid of linear equations of planar (2-D) motion. It is interesting that most of the nonlinear equations, which began appearing in the 1980s, are for

---

*Corresponding author. Tel.: +1 514 398 6294; fax: +1 514 398 7365.

E-mail address: mary.fiorilli@mcgill.ca (M.P. Païdoussis).

[1]The early theoretical models were linear, while 3-D motions are inherently associated with nonlinear effects, as is clear from the equations of motion derived in Part 1 (Wadham-Gagnon et al., 2007).

three-dimensional (3-D) motions [e.g., by Lundgren, Sethna and Bajaj (1979), Bajaj et al. (1980), and Rousselet and Hermann (1981)], although some others were for 2-D motions [e.g., Ch'ng and Dowell (1979), Semler et al. (1994)].

The theoretical and experimental work of Lundgren et al. (1979) may be said to have kindled researchers' interest in the 3-D dynamics of pipes conveying fluid. The system, involving a cantilevered pipe fitted at the free end with an inclined nozzle, was found to lose stability either in the plane of the nozzle or perpendicular to it, in multiple interspersed ranges of β.[2] Rousselet and Herrmann's (1981) results show that in these same ranges of β the effect of nonlinearities is either destabilizing or stabilizing [see Païdoussis (1998, Section 5.7.1)].

The definitive work on 3-D nonlinear dynamics of plain cantilevered pipes conveying fluid was done by Bajaj and Sethna (1984), making use of centre manifold and normal form techniques. Once again, it was found that the system loses stability and develops either planar or 3-D (orbital or rotary) flutter in multiple interspersed ranges of β—but not the same ranges as those discussed in the foregoing. This work was later extended to pipes with imperfections (Bajaj and Sethna, 1991), showing that flutter can (i) remain in a plane, (ii) start as planar and then become orbital, or (iii) display complex spatial transients and more complex dynamics.

Finally, we come to the topic of nonlinear motions of cantilevered pipes with an end-mass, the very topic of this paper. Work on this subject has been done by Copeland and Moon (1992), Semler and Païdoussis (1995) and Païdoussis and Semler (1998). Here, a brief review is given, while a fuller version is provided in Païdoussis (1998, Section 5.8.3).

Copeland and Moon's (1992) experimental findings were very interesting and provided the impetus for further work in this area. The experiments were conducted with particularly long ($L = 0.989$ m, $L/D_i = 124$, $D_o/D_i \simeq 2$; L, D_o and D_i being the length, external and internal diameters, respectively) vertically hanging, elastomer cantilevered pipes, fitted at the free end with end-masses of different sizes. A particularly rich dynamical behaviour was obtained, as summarized in Fig. 1.

In Fig. 1, $\Gamma = m_e/[(M + m)L]$, where m_e is the end-mass, M the mass of the fluid per unit length, and m that of the pipe per unit length; $u_g = U/(gL)^{1/2}$ is the dimensionless flow velocity used by Copeland and Moon.[3] In addition to planar and orbital (rotary) motions, an extraordinary array of geometrically more complex motions was discovered. In all cases with $\Gamma \neq 0$, for sufficiently high u_g the motions became chaotic, often with several intervening periodic oscillation states. In at least some cases, the quasiperiodic route to chaos was found to be followed. The plain cantilever proved to be a singular case, where planar flutter persists to the maximum flow available, with no secondary bifurcations. In these experiments, $\beta = 0.219$; yet the observed flutter was planar, which does not agree with Bajaj and Sethna's (1984) predictions for horizontal cantilevers, most probably because of the importance of gravity in these experiments.

Païdoussis and Semler (1998) studied both theoretically and experimentally the dynamics of more modestly long ($L/D_i = 74$) hanging elastomer cantilevers. In these experiments, $\beta = 0.125$–0.150, where, according to Bajaj and Sethna, flutter should be (and in fact was observed to be) planar immediately after the Hopf bifurcation; the end-mass parameter was in the range $\Gamma = 0.023$–0.380—considerably smaller than in Copeland and Moon's experiments.

Interesting observations were made in this case also. Planar flutter was followed by a secondary bifurcation as the flow velocity was increased, which could be identified with a sudden and substantial increase in the frequency, accompanied by a peculiar mode of oscillation with a seemingly stationary node around the mid-length. For higher flow velocities, the motion eventually became chaotic and 3-D.

Païdoussis and Semler's (1998) experimental results were compared to the theoretical ones, obtained with their 2-D model and by using 4 beam modes in the Galerkin solution scheme. The Hopf and secondary bifurcations were reasonably well predicted ($u_{th} = 4.66$ versus $u_{exp} = 4.8$ for the Hopf bifurcation, and $u_{th} = 7.26$ versus $u_{exp} = 7.6$ for the secondary one, in a typical case with $\Gamma = 0.15$), as was the transition to chaos ($u_{th} = 8.76$ versus $u_{exp} \simeq 8.0$).

An additional, interesting study was conducted by Semler and Païdoussis (1995), in which, instead of an end-mass, there was a mass defect at the free end of a cantilever ("negative end-mass"). After the Hopf bifurcation, and a symmetry-breaking pitchfork bifurcation, the system was shown to undergo a period doubling. Then, it became chaotic, following, in textbook fashion, the type I intermittency route to chaos.

From the foregoing it is quite clear that, if the 3-D dynamics of a cantilevered pipe is interesting, it becomes much richer and even more interesting in the presence of an end-mass. Hence work in this area has continued, notably by deriving a 3-D version of the nonlinear equations of motion of Semler et al. (1994) in Part 1 of this work (Wadham-Gagnon et al., 2007). These equations have been used to study the 3-D behaviour of a pipe with an end-mass. Typical dynamical behaviour for such a system is presented in Section 2 for two different values of the end-mass parameter. In Section 3, the effect of the number of beam modes used in the Galerkin discretization is studied by carrying out

---

[2]As defined in Part 1 (Wadham-Gagnon et al., 2007), $\beta = M/(M + m)$, where M is the mass of the conveyed fluid per unit length, and m is the mass of the pipe per unit length.

[3]In the analytical part of the study, which was not wholly successful (Copeland, 1992), the long vertical pipes were modelled as hanging strings.
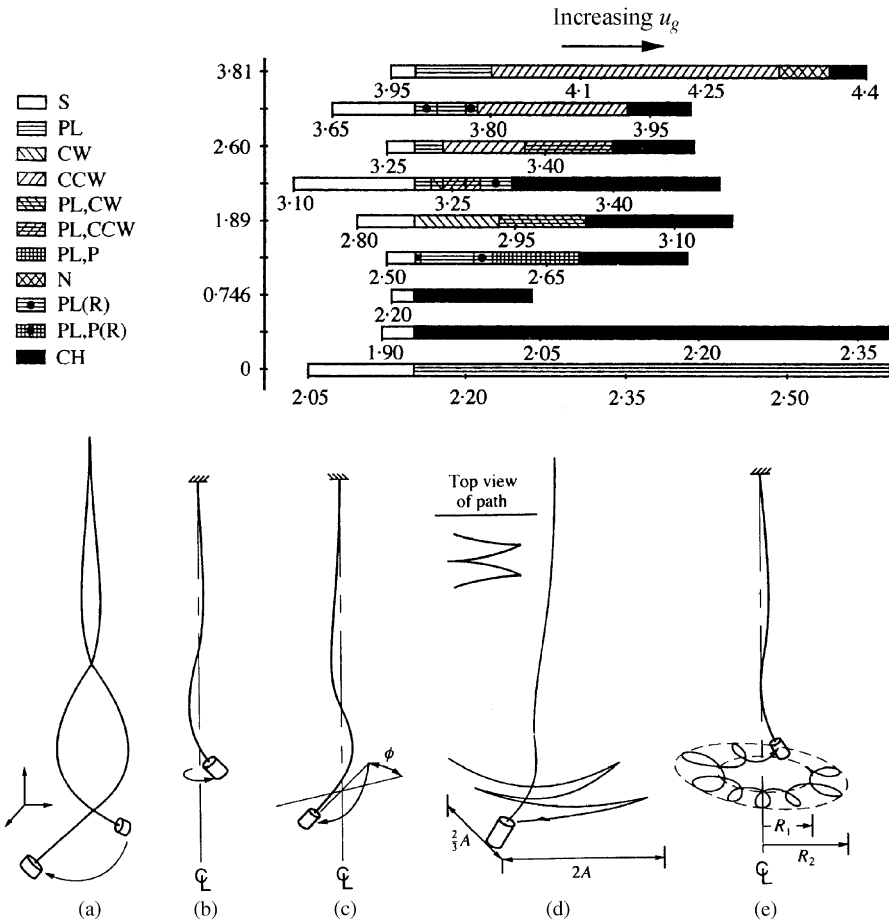
Fig. 1. Transition from equilibrium to chaos for 3-D motions of the system for various end-masses. Top: the ranges of various oscillatory states in terms of increasing u_g for different end-masses, Γ. S: stationary tube; PL: planar oscillation; CW: clockwise rotating motion; CCW: counter-clockwise rotating motion; PL, CW: clockwise rotating planar oscillation; PL, CCW: counter-clockwise rotating planar oscillation; PL(R): planar oscillation rotating through a finite angle; PL, P: coupled planar and pendular oscillation; PL, P(R): coupled oscillation and pendular oscillation rotating through a finite angle; N: nutation; CH: chaos. Bottom: sketches of various periodic motions: (a) PL; (b) CCW; (c) PL(R); (d) PL, P; (e) N [Copeland and Moon, 1992].

convergence tests, showing that at least 6 beam modes in each direction (y and z) are necessary for the results to converge; for larger end-masses, or for longer pipes, more modes are necessary to attain convergence. Then, the theoretical results are compared with the experimental ones in Section 4 and, as will be seen, good agreement is achieved, both qualitatively and quantitatively.

2. Typical dynamics of a cantilevered pipe with an end-mass

2.1. The equations of motion

The equations of motion have been derived in Part 1 of this work. They are given therein as Eqs. (40) and (41); for the work here, all terms related to the "intermediate springs" should be deleted. The dimensionless form of these equations is as in Eqs. (43) and (44) of Part 1, again with all the κ terms deleted. These equations will not be repeated here for brevity. However, some of the key dimensionless parameters are given again for convenience, as follows:

$$u = \left(\frac{M}{EI}\right)^{1/2} UL, \quad \gamma = \left(\frac{m+M}{EI}\right) L^3 g, \quad \beta = \frac{M}{m+M}, \quad \Gamma = \frac{m_e}{(m+M)L}, \quad \omega = \left(\frac{m+M}{EI}\right)^{1/2} L^2 \Omega, \tag{1}$$

where u is the dimensionless flow velocity, γ the dimensionless gravity parameter, β a mass parameter, Γ the dimensionless end-mass parameter, and ω is the dimensionless frequency of oscillation. The dimensional quantities involved are M and m, the mass of the conveyed fluid and that of the empty pipe per unit length, respectively, EI, the pipe flexural rigidity, L, the pipe length, g, the acceleration due to gravity, m_e, the added end-mass, U, the flow velocity, and Ω, the radian frequency of oscillation.

Following the method of solution described in Part 1 (Section 7), the dimensionless set of nonlinear partial differential equations is discretized by Galerkin's technique with the eigenfunctions of a plain cantilever beam as the base functions. A discussion on the necessary number of beam modes used in the discretization is given in Section 3. The resulting set of ordinary differential equations is then solved by Houbolt's finite difference method [see Semler et al. (1996) for details on Houbolt's finite difference method].

2.2. Results for $\Gamma = 0.1$

The dynamics of a typical system is considered, to illustrate the rich dynamical behaviour that can be obtained. The numerical values of the physical parameters were chosen to correspond to those of a system used in the experiments described in Païdoussis and Semler (1998), as given in Table 1. The corresponding dimensionless parameters are given in Table 2. For this system, the ratio of dimensional to nondimensional flow velocity, $U/u = 1.087$ m/s.

The bifurcation diagram for this system showing the dimensionless displacement of the tip (free-end) versus dimensionless flow velocity, u, is shown in Fig. 2. The dimensionless displacement in the y-direction is η and the dimensionless displacement in the z-direction is ζ; the total dimensionless tip-displacement of the pipe being the resultant of these two. To construct this bifurcation diagram, at least 6 Galerkin modes in each direction are necessary for $u < 9$ and 8 modes for $u \geqslant 9$ refer; to the convergence tests described in Section 3.

The system is stable until the threshold of the Hopf bifurcation at $u \simeq 5.4$. The ensuing flutter is planar up to $u = 8.0$, in the plane determined by the initial conditions, which are not necessarily in the y (dimensionless η) or z (dimensionless ζ) direction. Fig. 3 shows (a) a time trace, (b) a phase-plane plot, (c) a top view of the tip displacement, and (d) a PSD plot for $u = 7.8$; the PSD plot shows a dimensionless fundamental frequency of $f = 2.95$ (in cycles per dimensionless second), along with harmonics, for the oscillations.

In the velocity range $u = 8.0$–8.5, the oscillation becomes quasiperiodic, as illustrated in Fig. 4 (for the same set of plots as in Fig. 3) for $u = 8.2$; the motion still remains planar. The fundamental frequencies are seen to be $f_1 = 0.9$ and $f_2 = 3.05$. All the other frequency peaks in the PSD plot can be expressed as linear combinations of these two fundamental frequencies (e.g., $f_3 = 2f_2 - f_1$ and $f_4 = 2f_2 + f_1$).

As u is increased further, there is a return to periodic flutter for $u = 8.6$–9.5, as shown in Fig. 5 for $u = 9.0$. This return to periodic oscillation is characterized by a "jump" in the dominant frequency, from $f \simeq 3$ at $u = 8.5$ to $f \simeq 6.4$ at $u = 8.6$, as well as by a reduction in the amplitude. The bifurcation diagram of Fig. 2 shows very clearly the change in the amplitude at $u = 8.6$.

The spatial shape of the pipe in the course of a period of oscillation before and after this frequency jump is illustrated in Fig. 6. Fairly near the onset of flutter, namely at $u = 6$, the pipe has relatively small amplitude and undergoes mainly

Table 1
Pipe parameters used in the calculation

Length, L	0.443 m
Inner/outer diameter, D_i/D_o	6.4/15.7 mm
Flexural rigidity, EI	7.42×10^{-3} N m^2
Density of the pipe, ρ_p	1167 kg/m^3
Density of the fluid, ρ_f	999 kg/m^3
Mass per unit length of pipe, m	0.189 kg/m
Mass per unit length of fluid, M	0.0320 kg/m

Table 2
Dimensionless parameters used in the calculation

Dimensionless mass parameter, β	0.145
Dimensionless gravity parameter, γ	25.4
Dimensionless end-mass parameter, Γ	0.1
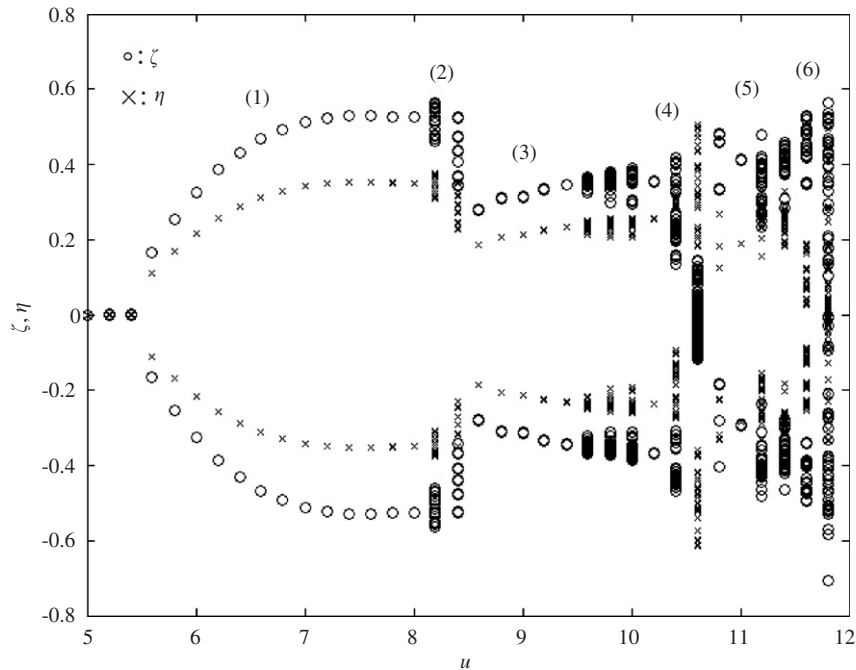
Fig. 2. Bifurcation diagram for the pipe with an end-mass obtained with $\Gamma = 0.1$, $\beta = 0.145$, $\gamma = 25.4$; showing the nondimensional tip displacements in the y- and z-direction: (1) planar flutter, $u = 5.4$ to 8.0; (2) planar, quasiperiodic oscillations, $u = 8.0$–8.5; (3) frequency jump and return to periodic flutter, $u = 8.6$–9.5; (4) three-dimensional chaotic oscillations, $u = 10.6$ then $u = 11.8$; (5) three-dimensional period-3, planar period-1 and chaotic oscillation, sequentially, $u = 10.8$–11.5; (6) quasiperiodic, three-dimensional oscillations, $u = 11.6$.

first- and second beam-mode oscillations (Fig. 6(a)), with a strong second-beam mode travelling-wave component; this is followed by larger amplitude oscillations of similar basic shape at $u = 7.8$ (Fig. 6(b)). At a flow velocity greater than the critical flow velocity for the jump in frequency ($u = 9$), the pipe has mainly second beam-mode shape of a significantly different basic oscillation form; a fixed point (node) exists near the middle of the pipe, and the amplitude of the oscillations is clearly reduced *vis-à-vis* $u = 7.8$ (Fig. 6(c)). If one were to focus on the evolution of the oscillations of the mid-point of the pipe, the reduction in the amplitude associated with the frequency jump is much more pronounced compared to that for the oscillation of the tip, on which the discussion in this paper is focused. The maximum amplitude of the tip changes from $0.64L$ before the jump in frequency to $0.37L$ after the jump, indicating around a 40% reduction in the amplitude; while the amplitude of the mid-point is reduced from $0.23L$ to $0.07L$, which is equivalent to nearly a 70% reduction.

The pipe shape after the frequency jump is very similar to that observed in Part 2 (Païdoussis et al., 2007) for Case 1. An analogy can also be made with a fluttering flag of different lengths (Païdoussis, 2003, Section 10.3.6(b)), where a frequency jump is observed as the length of the flag increases.

The high-frequency oscillation of the pipe becomes quasiperiodic at $u = 9.8$, and then chaotic at $u = 10$ (Fig. 6(d)). This chaotic motion is followed by planar high-frequency periodic oscillations and then again planar chaotic motion. The first signs of three-dimensionality appear at $u = 10.6$, where 3-D chaotic motion is observed. With a further increase in u, the 3-D chaotic motion becomes 3-D period-3 oscillation, as seen in the time traces and the ζ versus η plots of the tip displacement of Fig. 7 for $u = 10.8$ (note the three heavier attracting trajectories). It is interesting to note that the solution for $u = 10.8$ is planar for a long nondimensional time ($\tau < 50$) before it finally converges to 3-D period-3 oscillations; the plots in Fig. 7 are for $\tau > 50$ where the oscillations are 3-D. The period-3 oscillation becomes planar high-frequency period-1 oscillation at $u = 11$ (similar to that at $u = 9$), and then again planar chaotic motion for $u = 11.4$ (Fig. 8), followed by 3-D quasiperiodic motion at $u = 11.6$ and then 3-D chaotic motion at $u = 11.8$ (Fig. 9). In Figs. 8 and 9, the Poincaré maps show the velocity versus displacement of the tip in the y-direction when the velocity of the tip in the z-direction is zero. The cluster of points in the $\{\dot{\eta}, \eta\}$ – plane clearly shows that the oscillation is chaotic, rather than, say, quasiperiodic. It is interesting to note that in the case of planar motion (Fig. 8) we have two separate
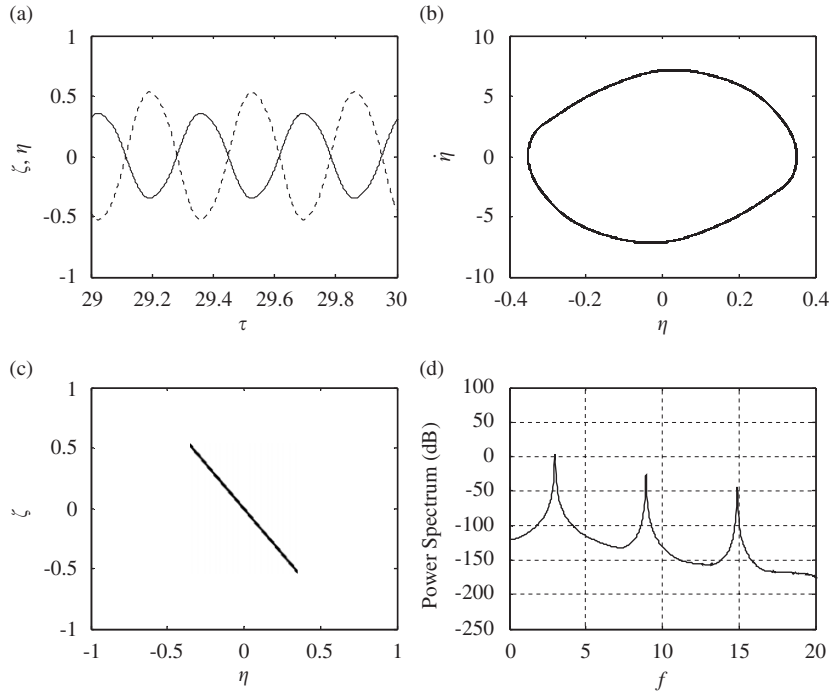
Fig. 3. Planar flutter for the system of Fig. 2 ($u = 7.8$; flow region 1): (a) time trace of ζ (dotted line) and η (continuous line) displacements for the pipe with an end-mass, (b) phase plane diagram, (c) tip displacement of the pipe, illustrating the plane of motion, and (d) PSD plot showing that the fundamental dimensionless frequency is at $f = 2.95$.
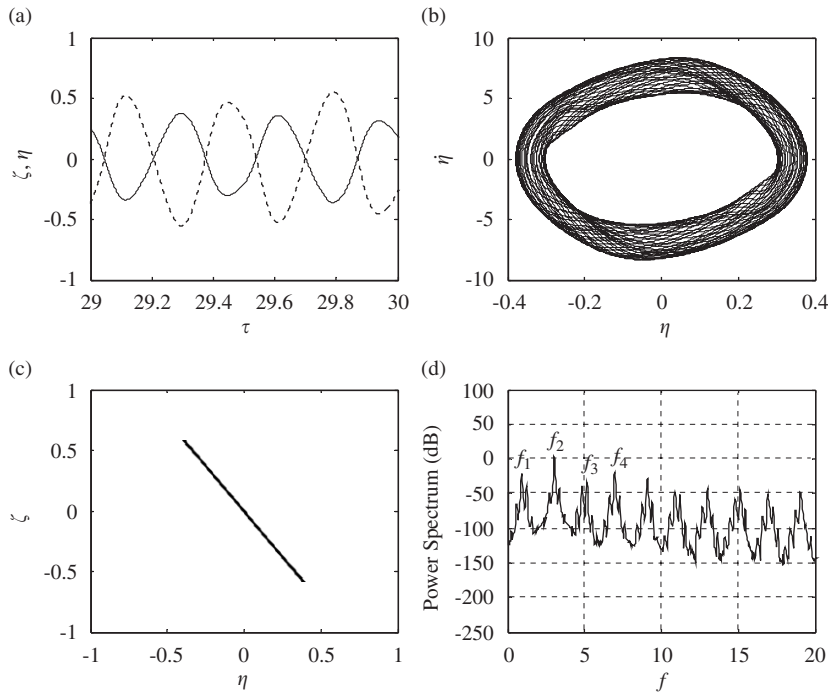
Fig. 4. Quasiperiodic planar flutter for the system of Fig. 2 ($u = 8.2$; flow region 2): (a) time trace of ζ and η displacements for the pipe with an end-mass, (b) phase plane diagram, (c) tip displacement of the pipe, illustrating the plane of motion, and (d) PSD plot showing dimensionless fundamental frequencies $f_1 = 0.9$ and $f_2 = 3.05$.
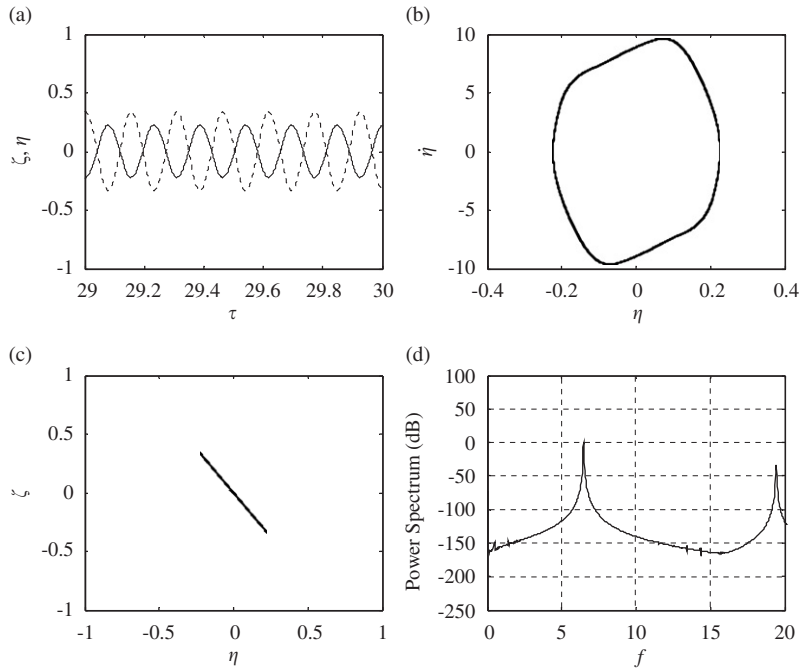
Fig. 5. Planar high-frequency flutter for the system of Fig. 2 ($u = 9.0$; flow region 3): (a) time trace of ζ and η displacements for the pipe with an end-mass, (b) phase plane diagram, (c) tip displacement of the pipe, illustrating the plane of motion, and (d) PSD plot showing dimensionless fundamental frequency $f = 6.4$.
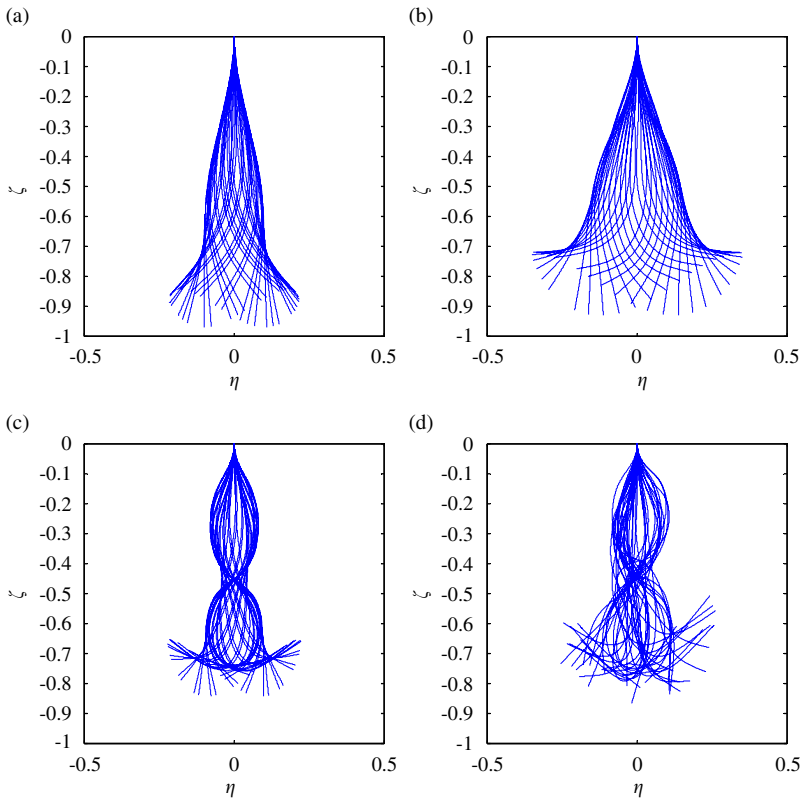
Fig. 6. The shape of the oscillating pipe: (a) $u = 6.0$, $f = 2.7$, (b) $u = 7.8$, $f = 2.95$, (c) $u = 9.0$, $f = 6.45$, (d) $u = 10$, chaotic.
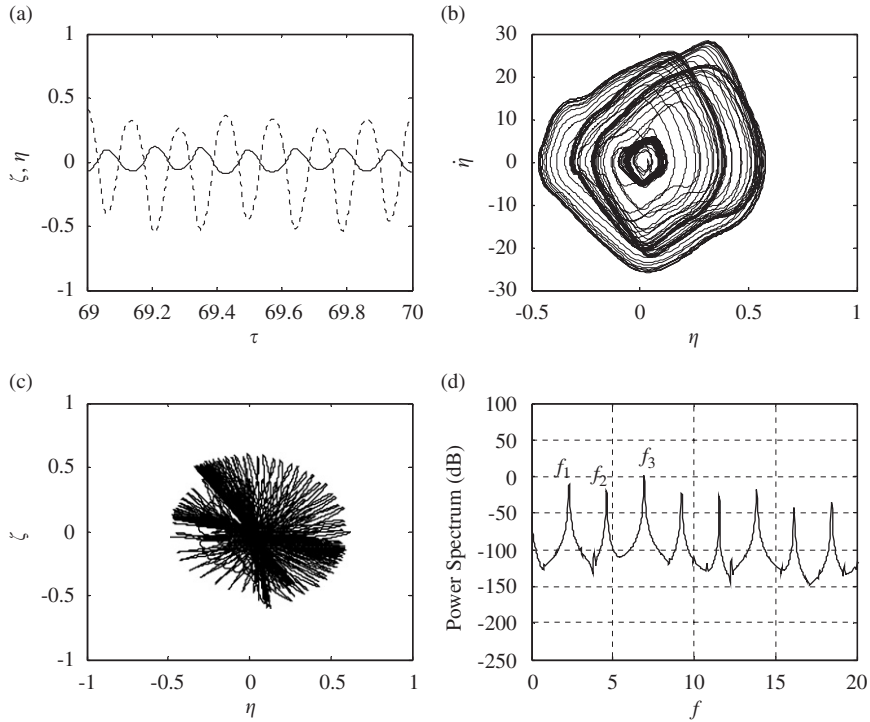
Fig. 7. Three-dimensional period-3 flutter for the system of Fig. 2 ($u = 10.8$; flow region 5): (a) time trace of ζ and η displacements for the pipe with an end-mass, (b) phase plane diagram, (c) tip displacement of the pipe, and (d) PSD plot showing dimensionless frequencies $f_1 = 2.3$, $f_2 = 4.6$ and $f_3 = 6.9$.
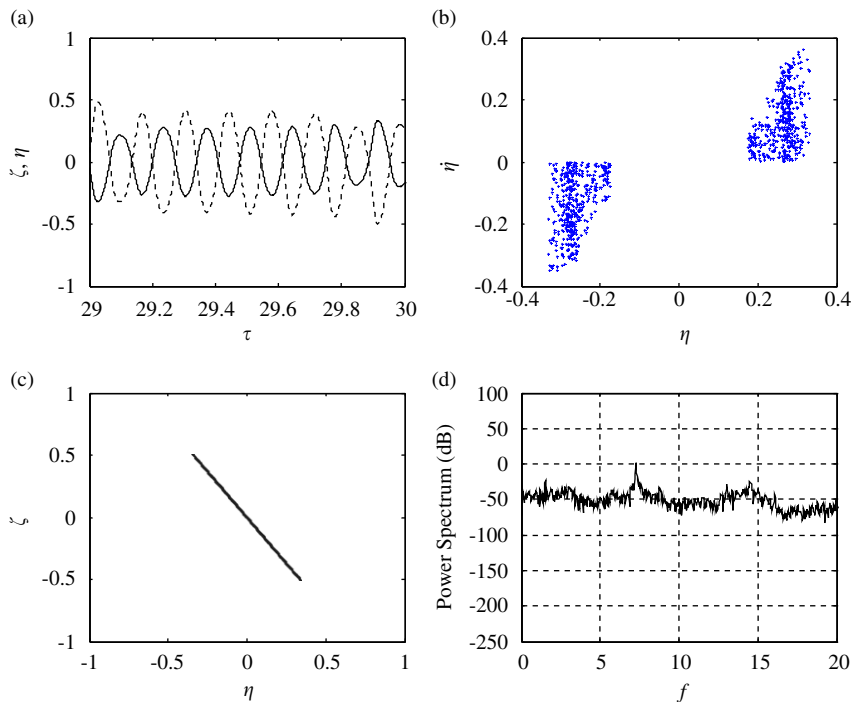
Fig. 8. Planar chaotic oscillation for the system of Fig. 2 ($u = 11.4$; flow region 5): (a) time trace of ζ and η displacements for the pipe with an end-mass, (b) Poincaré map, (c) tip displacement of the pipe, illustrating the plane of motion, and (d) PSD plot.
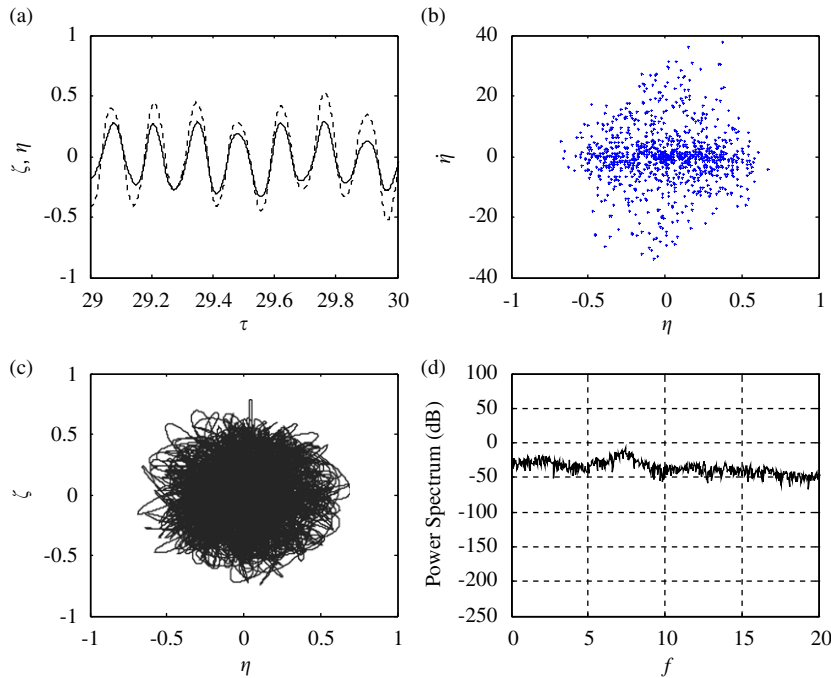
Fig. 9. Three-dimensional chaotic oscillation for the system of Fig. 2 ($u = 11.8$): (a) time trace of ζ and η displacements for the pipe with an end-mass, (b) Poincaré map, (c) tip displacement of the pipe, and (d) PSD plot.

clusters, while for the 3-D motion (Fig. 9) we have one, centrally located. However, there is no deeper meaning to this; if a different "trigger" had been used for plotting the points, the shape of the clusters could have been dramatically altered, but not the general character of the Poincaré map (characterizing a chaotic motion).

Now that the results of Figs. 2–9 have been presented, it is of interest to mention that, to construct the bifurcation diagram of Fig. 2, nonzero initial conditions have been used in both the η and ζ (y and z) directions. If one uses zero initial conditions in, say, the η direction, the resulting motion will be along ζ direction! Then, in the bifurcation diagram, the η-curve will totally disappear.

As mentioned before, Païdoussis and Semler (1998) analysed the 2-D model of this system by using 4 Galerkin modes. We shall now undertake a comparison between the 3-D results discussed above and those of the earlier, 2-D analysis. We reconstructed the bifurcation diagram for the 2-D problem, this time by using 8 Galerkin modes, to be able to compare the 2-D results with the 3-D ones in this paper for the same number of modes. As expected, the results before the onset of 3-D oscillations are exactly the same in the 2-D and 3-D solutions. According to the 3-D results, the first signs of three-dimensionality appear at $u = 10.6$, where a 3-D chaotic oscillation occurs. According to the 2-D model, the motion at this flow velocity is period-4! The 3-D period-3 motion at $u = 10.8$ is replaced by a 2-D period-3 motion in the 2-D model. At higher flow velocities, when according to the 3-D results, the pipe undergoes planar oscillation, the two models are in agreement again. At $u = 11.6$, 3-D quasiperiodic oscillation arises, followed by 3-D chaos. The 2-D model, on the other hand, cannot predict any solution for this range of flow velocities, i.e., the finite difference scheme does not converge. This comparison between 2-D and 3-D model predictions makes it clear that, when the motion is 3-D, to obtain the correct dynamical behaviour, even qualitatively, requires the use of the 3-D model. On the other hand, because 2-D motions in this system persist to relatively high flow velocities, the dynamical behaviour can be predicted well enough by the 2-D model up to $u = 10.4$.

2.3. Results for $\Gamma = 0.15$

In this section, the dynamics of a system with different system parameters is investigated to ascertain whether the results predicted in Section 2.2 are particular to that set of parameters or are broadly generic. The nondimensional
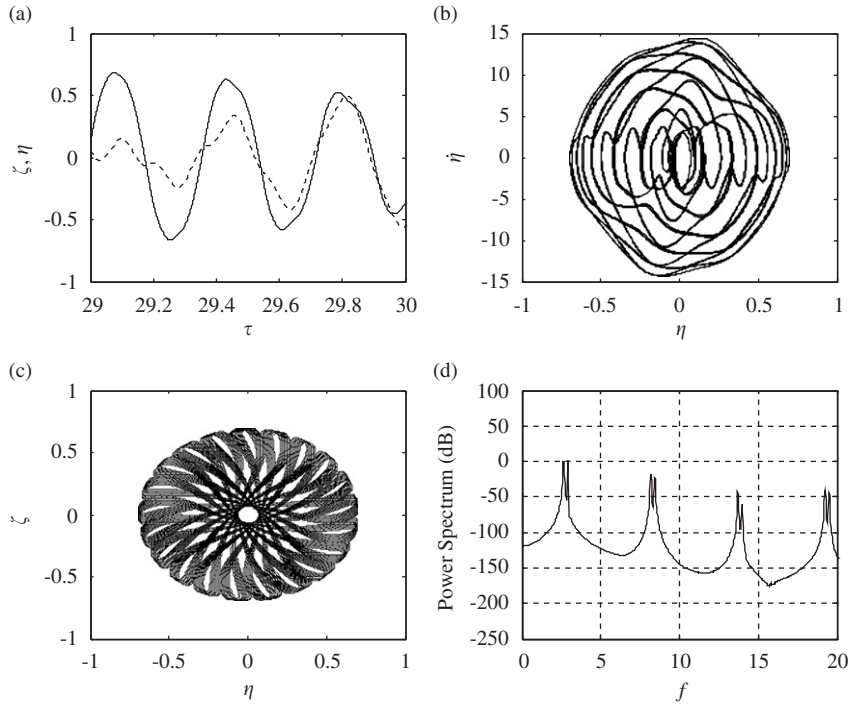
Fig. 10. Three-dimensional quasiperiodic oscillation for the system with $\Gamma = 0.15$, $\beta = 0.147$, $\gamma = 19.8$ ($u = 7$): (a) time trace of ζ and η displacements for the pipe with an end-mass, (b) phase plane diagram, (c) tip displacement of the pipe, and (d) PSD plot.
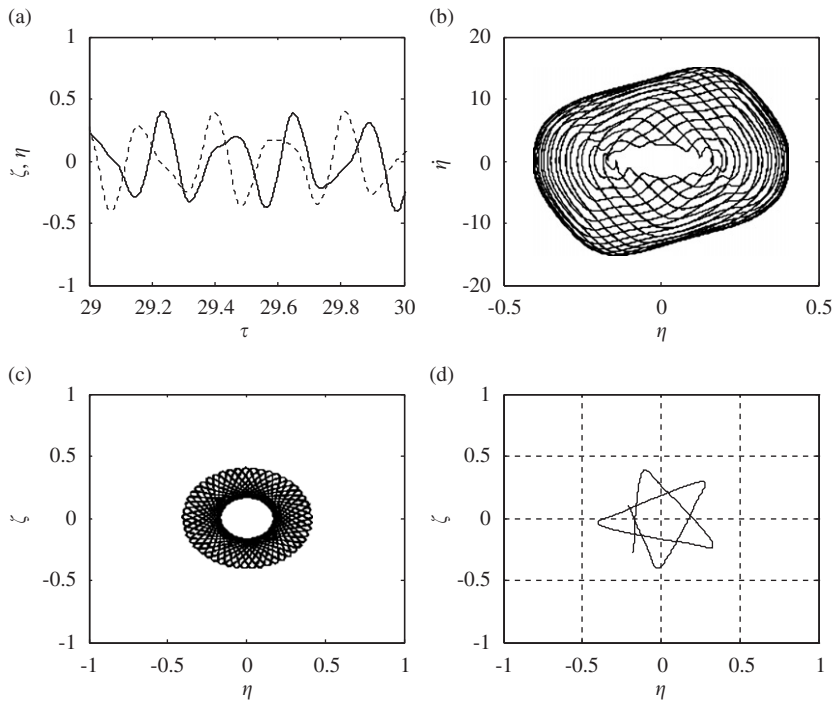
Fig. 11. Three-dimensional quasiperiodic oscillation for the system with $\Gamma = 0.15$, $\beta = 0.147$, $\gamma = 19.8$ ($u = 8.8$): (a) time trace of ζ and η displacements for the pipe with an end-mass, (b) phase plane diagram, (c) tip displacement of the pipe, and (d) the perambulating 5-pointed star; the structure of the pattern in (c) obtained from a simulation over a short time-span.

parameters used here are: $\gamma = 18.9$, $\beta = 0.145$ and $\Gamma = 0.15$. Thus, β is the same as for the system of Section 2.2, and γ is but a little different[4]; the main difference is in the parameter Γ, which here is 50% larger.

A larger end-mass makes the pipe unstable at lower flow velocities compared to the previous case. The critical point for the Hopf bifurcation is at $u = 4.8$ (versus $u = 5.4$ in the previous case), after which a planar periodic oscillation arises with a frequency of $f = 2.5$ (in cycles per dimensionless second). At $u = 6.6$, the first signs of three-dimensionality appear with the onset of quasiperiodic motions. The peak in the PSD plots is still around $f = 2.5$. Fig. 10 shows the motion of the pipe at $u = 7$. At this flow velocity, the structure of the 3-D motion of the pipe is basically a nearly planar motion, which changes its angle in every "quasi-cycle" of oscillation to produce the aesthetically pleasing pattern of Fig. 10(c). The 3-D quasiperiodic motion is followed by 3-D chaotic oscillation at $u = 7.4$, which persists until $u = 7.8$ where a planar periodic motion begins with a frequency of $f = 3$, followed by a 3-D quasiperiodic oscillation at $u = 8.8$ with a frequency peak at $f = 4.8$ (Fig. 11). At this flow, a jump in the amplitude of the oscillation is clear in the bifurcation diagram (not shown here for brevity). Fig. 11(d) shows the ζ versus η plot of the tip displacement of the pipe at $u = 8.8$ for only one cycle of oscillation. As can be seen, the pattern of cross-sectional motion is that of a five-pointed star, which repeats itself every "quasi-cycle" of oscillation, but with a small change in the angle, producing the pattern shown in Fig. 11(c) after many cycles. The oscillations become chaotic at $u = 9.4$ and remain chaotic thereafter.

It is concluded that the general behaviour of the system is not very dramatically different from that of Section 2.2 (which has been studied extensively in this paper), even though Γ was increased by 50%.

To obtain the solutions for this system, in view of the convergence tests described in the next section, at least a 6-mode analysis was found to be necessary for $u < 8.5$ and an 8-mode analysis for $u \geqslant 8.5$.

3. On convergence with increasing number of Galerkin modes

As mentioned in Section 2, the equations of motion describing the motion of a pipe with an end-mass are discretized by Galerkin's technique with the eigenfunctions of a cantilever beam as basis functions. A very important issue is to make sure that a sufficient number of beam-modes is used in the discretization to obtain reliable results. The critical flow velocities for the different bifurcations as well as the amplitude of oscillations are checked in the convergence tests to be discussed.

Table 3 shows the critical values of the flow velocity for $\gamma = 25.4$, $\beta = 0.142$ and $\Gamma = 0.1$, found using different numbers of modes. The first row gives the number of modes used in the y- and z-direction: for example, "4" means that 4 modes in the y-direction and 4 modes in the z-direction have been used. This table shows that by using 8 modes the results have converged, in the sense that the values do not change anymore if the number of Galerkin modes is increased further. Moreover, as one uses more modes, the numerical solution of the resulting set of ordinary differential equations converges[5] for a wider range of flow velocities; e.g., by using 4 modes in each direction, no solution can be found for $u > 10.2$ because the finite difference scheme does not converge, while by using 8 modes in each direction, solutions can be found for flow velocities up to $u = 12$.

The other necessary test is to look at the amplitudes in the results and see if they converge to a particular value as the number of modes is increased, or not. This test has also been conducted (not shown here for the sake of brevity) and the result is that, to find the converged solutions, one has to use at least 6 modes for $u < 9$ and 8 modes for $u \geqslant 9$. Of course, one can always use more modes; but this means solving a larger set of ordinary differential equations, which of course requires more computational time. To guarantee convergent results, some time-consuming 10-mode calculations were conducted for selected flow velocities in the range of interest. The results of these calculations are exactly the same as those produced by using 8 modes in each direction, assuring us that the results obtained by using 8 modes have converged. Using only 4 beam modes in each direction, the tip-amplitude of the pipe was found to be greater than the pipe length for some flow velocities: an obviously non-physical situation.

As an example of the effect of the number of Galerkin modes used in the calculation, let us concentrate on the results for $u = 9.5$. The 4-mode calculations converge to a 3-D chaotic solution, while by using 6 modes, one finds quasiperiodic planar motion, and by using 8 modes, high-frequency periodic planar motion! The 10-mode calculation results in a high-frequency periodic planar motion as well, thus confirming the result of the 8-mode calculation.

The same convergence test was conducted for the second case discussed in Section 2.3 showing that at least 6 modes in each direction are necessary for $u < 8.5$ and 8 modes in each direction thereafter, to achieve convergence in the results.

---

[4]In fact, it has been shown that this difference has a negligible effect on the dynamics of the system; the bifurcation diagram of the system with $\Gamma = 0.1$ and $\gamma = 18.9$ was produced (not shown here) and the results are very similar to those presented in Section 2.2.

[5]Note that "convergence" has two different meanings in this paragraph: convergence of the results in the Galerkin sense as modes are added in the discretization of the PDEs, and convergence of the finite difference scheme used to solve the resulting set of ODEs.

Table 3
Effect of number of Galerkin modes in the theoretical calculations

Number of modes	4	6	8	10
Hopf bifurcation	5.4	5.4	5.4	5.4
Onset of quasiperiodic oscillations	8.2	8.2	8.2	8.2
Critical flow velocity for the jump in frequency	8.5	8.6	8.6	8.6
Onset of 3-D chaos	8.8	10.4	10.6	10.6
No convergence	10.2	11.4	12	—

Table 4
Critical flow velocities: theory versus experiment

	u		f (Hz)	
	Experiment	Theory	Experiment	Theory
Hopf bifurcation	5.2	5.4	2.8	2.75
Jump in frequency	7.7	8.6	4.3	6.0
Chaos	8	10	—	—

4. Comparison with experimental observations

Experiments by Païdoussis and Semler (1998) were conducted with the same elastomer pipes and roughly the same mass parameter, β, and gravity parameter, γ. For the range of end-masses tested ($0 < \Gamma < 0.4$), the first bifurcation was of the Hopf type, leading to planar flutter. In some cases (more precisely when $\Gamma > 0.06$), the pipe would undergo a second bifurcation characterized by a jump in frequency and reduction in the amplitude of oscillation. Before this second bifurcation, travelling wave oscillations were observed. Immediately following the frequency jump, the oscillations were seen to have a seemingly fixed node near the middle of the pipe. By increasing the flow velocity further, chaotic and 3-D oscillations were observed. Clearly, these observations are in qualitative agreement with those in the theoretical results discussed in Section 2.2, except for the small window of quasiperiodic oscillations for $8 < u < 8.5$ in the theoretical results, which were not observed in the experiments. The critical values observed in the experiment together with the corresponding theoretical results are summarized in Table 4 for $\gamma = 25.4$, $\beta = 0.142$ and $\Gamma = 0.1$.

The theoretical results are therefore also in reasonably good quantitative agreement with the experimental observations. The onset of the periodic oscillations (Hopf bifurcation point) is at $u = 5.2$ in the experimental results and at $u = 5.4$ according to the theoretical results. In the experiments as well as in the theoretical results, the oscillations are planar after the Hopf bifurcation for a range of flow velocities. The theory predicts the jump in frequency around $u = 8.6$, from 2.75 to 6.0 Hz, and the amplitude of the tip oscillations decreases from $0.64L$ to $0.37L$. In the experimental observations, the jump in frequency occurs at $u = 7.7$, and the frequency changes from 2.8 to 4.3 Hz. Also, the theoretical results show a node at the mid-point of the cylinder for the after-jump values of the flow velocities (Fig. 6(c)), in agreement with the observed experimental results. Chaotic and 3-D oscillations start at $u = 10$ according to the theoretical results, while in the experiments the chaotic oscillations have been observed to begin around $u = 8$.[6]

In all cases, the critical flow velocities seen in the experiments are smaller than those predicted by the theoretical results. A possible reason for this could be the existence of minor imperfections in the pipes used in the experiments. Another possible reason is the fact that the end-masses used in the experiments are of finite dimension as opposed to the point-mass modelled in the theory.

---

[6]When the experiments were conducted, there was no 3-D theory available and hence the study of the detailed dynamical behaviour for u substantially higher than $u = 8$ was not pursued.

5. A brief note on the dynamics of long pipes with an end-mass

If a vertically hanging pipe is very long, then the large tension due to gravity renders the upper part of the pipe so stiff that, in the ensuing flutter at high enough flow velocities, only the lower part, near the free end, experiences substantial amplitude of oscillation.[7] In order to capture the dynamics of such a system with modal analysis, high enough modes with short enough wavelength must be considered.

The pipe employed in Copeland and Moon's (1992) experiments has a large gravitational coefficient, $\gamma = 295.27$ (it is recalled that $\gamma \sim L^3$), together with large end-mass parameters, $\Gamma = 0.37–3.81$. The critical flow velocities for dynamic instabilities are around $u = 20$, which is far greater than attainable in the experiments and in the theoretical calculations discussed in this paper. Following the discussion on convergence in Section 3, in order to have convergent results for such large flow velocities, the number of modes must be increased considerably, making the calculations cumbersome—in fact, effectively impossible with the resources available to the authors.

Although the main purpose of the present paper was not to deal with the very long pipes particularly, some calculations by using 8 beam-modes in each direction were conducted for selected values of Copeland and Moon's parameters. For the case with no end-mass, our theoretical results, in agreement with their observations, show planar oscillation after the loss of stability. For the two smallest end-mass parameters in Copeland and Moon's experiments, $\Gamma = 0.37$ and 0.746, we found that for increasing flow velocity, the stationary, equilibrium solution loses stability via a subcritical Hopf bifurcation (at $u = 11.74$ for $\Gamma = 0.37$ and at $u = 14.23$ for $\Gamma = 0.746$), which is followed by a torus bifurcation (at $u = 11.9$ for $\Gamma = 0.37$ and at $u = 14.5$ for $\Gamma = 0.746$), and at slightly higher flow velocity by chaos (at $u = 12.3$ for $\Gamma = 0.37$ and $u = 15$ for $\Gamma = 0.746$). Thus, the succession from periodic oscillations to chaos is very quick, in agreement with Copeland and Moon's experimental observations; the threshold of chaos for these two end-mass parameters in the experiments is $u = 15.6$ and 17.6, respectively. For larger values of the end-mass parameter (e.g., $\Gamma = 1.89$), the solutions (the lateral displacements of the pipe) converge to zero for small flow velocities, in agreement with the experimental observations; but, at higher flow velocities, where oscillatory motions have been observed experimentally, the solutions diverge very rapidly (i.e., no solutions could be obtained), which is here attributed to our inability to use a sufficient number of Galerkin modes in the calculations.

An alternative approach to overcome this problem could be to use other comparison functions when discretizing the nonlinear partial differential equations by Galerkin's technique. Eight-mode calculations were conducted using eigenfunctions found from the linear equation of motion in which the effect of the end-mass, gravity and partly the flow velocity were taken into account. Unfortunately, this again was not sufficient to obtain convergent results. Clearly, a different approach is needed; or, alternatively, sufficiently powerful computational hardware is required to allow calculations with 20, 30 or 50 modes.

6. Conclusion

In this paper, the 3-D nonlinear dynamics of a vertical cantilevered pipe with an end-mass has been studied by using the theoretical model developed in Part 1 of this three-part study (Wadham-Gagnon et al., 2007).

For a system studied previously also experimentally, as the flow velocity increases from naught, the hanging pipe loses stability by a Hopf bifurcation, indicating a travelling wave-form of oscillation. The periodic oscillation then undergoes another bifurcation, after which the frequency of oscillation increases dramatically. This jump in frequency is accompanied by a decrease in the amplitude of oscillations, together with the appearance of a stationary node at the mid-point of the pipe, giving a mainly second beam-mode shape to the oscillations. This is succeeded by quasiperiodic and then chaotic oscillations, all of the motions being planar up to this point. Then, the first signs of three-dimensionality appear, but the system oscillation becomes planar once again. Periodic and chaotic planar motions exist for a range of flow velocities until the 3-D quasiperiodic and chaotic motions start at higher flow velocities.

It was shown that by increasing the nondimensional flow velocity, one must use a larger number of beam modes when discretizing the set of partial differential equations by Galerkin's technique. Not using enough modes leads to unreliable and even erroneous results.

The theoretical results have been found to be in good agreement with the available experimental observations, both qualitatively and quantitatively. The experimental values for the critical flow velocities for the observed bifurcations are generally smaller than the theoretical values. This may be attributed to the existence of imperfections in the pipe used in the experiments, as well as because the end-mass is considered as a point-mass in the theory.

---

[7]A similar phenomenon has been observed for very long cantilevered (or pinned-free) cylinders subjected to external axial flow by Hansen and Ni (1976, 1979) and Ni and Hansen (1978); see Païdoussis (2003; Section 8.3.7(b)).

Finally, it has been found that for systems with very large Γ and γ parameters, such as those in Copeland and Moon's experiments, so many Galerkin modes are needed to obtain convergent results as to effectively put them beyond our current computational capabilities.

Taking the results of Parts 2 and 3 together, it is clear that the post-critical dynamics of the system (i.e., the dynamics beyond the threshold of the first instability) is very rich: two-dimensional (2-D) and 3-D oscillatory motions, periodic, quasiperiodic or chaotic, following loss of stability by either static divergence or flutter. Moreover, the bifurcations beyond the first one are often associated with distinctive changes in the modal form, amplitude and/or frequency of the motion.

To the extent possible, some of the theoretical results have been compared with experiments. Agreement is excellent in some cases, while it is merely acceptable in others. Reasons for this can be attributed both to physical imperfections in the experiments (e.g., with regard to uniformity of the pipe, mounting and attachment of the springs, unsteadiness of the flow velocity, etc.) and to weaknesses in the theoretical modelling (e.g., for very large motions, the equation of motion which is correct to $\mathcal{O}(\varepsilon^3)$ may be insufficient, the modelling of the attachment of the springs to the pipe, the assumption of a point end-mass, etc.).

It is clear that the work presented barely scratches the surface of this topic, even with the theoretical model and the experimental apparatus in their present state. It is felt that more systematic exploration of the parameter space, both theoretically and experimentally, will uncover even more interesting dynamics. In connection with Part 3, enhanced computational capability would permit exploring theoretically what has already been shown experimentally to be an exceptionally rich and fertile dynamical arena.

Acknowledgments

References

Bajaj, A.K., Sethna, P.R., 1984. Flow induced bifurcations to three-dimensional oscillatory motions in continuous tubes. SIAM Journal of Applied Mathematics 44, 270–286.

Bajaj, A.K., Sethna, P.R., 1991. Effect of symmetry-breaking perturbations on flow-induced oscillations in tubes. Journal of Fluid and Structures 5, 651–679.

Bajaj, A.K., Sethna, P.R., Lundrgren, T.S., 1980. Hopf bifurcation phenomena in tubes carrying fluid. SIAM Journal of Applied Mathematics 39, 213–230.

Benjamin, T.B., 1961a. Dynamics of a system of articulated pipes conveying fluid, I Theory. Proceedings of the Royal Society A 261, 457–486.

Benjamin, T.B., 1961b. Dynamics of a system of articulated pipes conveying fluid, II. Experiments. Proceedings of the Royal Society A 261, 487–499.

Bishop, R.E.D., Fawzy, I., 1976. Free and forced oscillations of a vertical tube containing a flowing fluid. Philosophical Transactions of the Royal Society (London) 284, 1–47.

Bourrières, F.-J., 1939. Sur un phénomène d'oscillation auto-entretenue en mécanique des fluides réels. Publications Scientifiques et Techniques du Ministère de l'Air, No. 147.

Copeland, G.S., 1992. Flow-induced vibration and chaotic motion of a slender tube conveying fluid. Ph.D. Dissertation. Cornell University, Ithaca, NY, USA.

Copeland, G.S., Moon, F.C., 1992. Chaotic flow-induced vibration of a flexible tube with end mass. Journal of Fluids and Structures, 6, 705–718 (also in American Society of Mechanical Engineers AMD-vol. 152, Proceedings International Symposium on Flow-Induced Vibration and Noise, vol. 8, pp. 63–77).

Ch'ng, E., Dowell, E.H., 1979. A theoretical analysis of nonlinear effects on the flutter and divergence of a tube conveying fluid. In: Chen, S.S., Bernstein, M.D. (Eds.), Flow-Induced Vibrations. ASME, New York, pp. 65–81.

Gregory, R.W., Païdoussis, M.P., 1966a. Unstable oscillations of tubular cantilevers conveying fluid—I. Theory. Proceedings of the Royal Society A 293, 512–527.

Gregory, R.W., Païdoussis, M.P., 1966b. Unstable oscillations of tubular cantilevers conveying fluid—II. Experiments. Proceedings of the Royal Society A 293, 528–542.

Hansen, R.J., Ni, C.C., 1976. An experimental study of flow-induced motions of flexible cables and cylinders aligned with flow direction. ASME Paper 76-WA/FE-15.

Hansen, R.J., Ni, C.C., 1979. Flow-induced motions of a flexible cable aligned with flow direction. IEEE Journal of Oceanic Engineering OE-4, 152–156.

Hill, J.L., Swanson, C.P., 1970. Effects of lumped masses on the stability of fluid conveying tubes. Journal of Applied Mechanics 37, 494–497.

Jendrzejczyk, J.A., Chen, S.S., 1985. Experiments on tubes conveying fluid. Thin Walled Structures 3, 109–134.

Lundgren, T.S., Sethna, P.R., Bajaj, A.K., 1979. Stability boundaries for flow induced motions of tubes with an inclined terminal nozzle. Journal of Sound and Vibration 64, 553–571.

Ni, C.C., Hansen, R.J., 1978. An experimental study of the flow-induced motions of a flexible cylinder in axial flow. ASME Journal of Fluids Engineering 100, 389–394 [Discussion 1979, 101, 202-293; 1980, 102, 119].

Païdoussis, M.P., 1963. Oscillations of liquid-filled flexible tubes. Ph.D. Thesis, University of Cambridge.

Païdoussis, M.P., 1970. Dynamics of tubular cantilevers conveying fluid. I. Mech. E. Journal of Mechanical Engineering Science 12, 85–103.

Païdoussis, M.P., 1998. Fluid–Structure Interactions: Slender Structures and Axial Flow, vol. 1. Academic Press, London.

Païdoussis, M.P., 2003. Fluid–Structure Interactions: Slender Structures and Axial Flow, vol. 2. Elsevier Academic Press, London.

Païdoussis, M.P., Semler, C., 1998. Non-linear dynamics of a fluid-conveying cantilevered pipe with a small mass attached at the free end. Journal of Non-Linear Mechanics 33, 15–32.

Païdoussis, M.P., Semler, C., Wadham-Gagnon, M., 2007. Dynamics of cantilevered pipes conveying fluid. Part 2: dynamics of the system with intermediate spring support. Journal of Fluids and Structures 23, this issue, doi:10.1016/j.j.fluidstructs.2006.10.009.

Rousselet, J., Hermann, G., 1981. Dynamic behaviour of continuous cantilevered pipes conveying fluid near critical velocities. Journal of Applied Mechanics 48, 943–947.

Semler, C., Païdoussis, M.P., 1995. Intermittency route to chaos of a cantilevered pipe conveying fluid fitted with a buoyant end-mass. Journal of Applied Mechanics 62, 903–908.

Semler, C., Li, G.X., Païdoussis, M.P., 1994. The non-linear equations of motion of pipes conveying fluid. Journal of Sound and Vibration 169, 577–599.

Semler, C., Gentleman, W.C., Païdoussis, M.P., 1996. Numerical solutions of second-order implicit ordinary differential equations. Journal of Sound and Vibration 195, 553–574.

Sugiyama, Y., Kawagoe, H., Kishi, T., Nishiyama, S., 1988. Studies on the stability of pipes conveying fluid (the combined effect of a spring support and a lumped mass). JSME International Journal Series 1 (31), 20–26.

Wadham-Gagnon, M., Païdoussis, M.P., Semler, C., 2007. Dynamics of cantilevered pipes conveying fluid. Part 1: Nonlinear equations of three-dimensional motion. Journal of Fluids and Structures 23, this issue, doi:10.1016/j.j.fluidstructs.2006.10.006.